Analytic Study on Long Wave Transformation over a Seamount with a Pit

Gang Wang[1,2]; Danjuan Fu[1,2]; Jinhai Zheng[1,2*]; Qiuhua Liang[2,3] and Yao Zhang[4]

[1] State Key Laboratory of Hydrology-Water Resources and Hydraulic Engineering, Hohai University, Nanjing 210098, China

[2] College of Harbour, Coastal and Offshore Engineering, Hohai University, Nanjing210098, China

[3] School of Civil Engineering and Geosciences, Newcastle University, Newcastle upon Tyne, NE17RU, United Kingdom

[4] National Marine Hazard Mitigation Service, Beijing 100194, China

Abstract: In this paper, an analytic solution is derived for linear long waves scattering over a submarine seamount landform with a pit. The seamount is axisymmetric with a pit on the top. The water depth is defined by a trinomial function in the radial direction. The governing linear shallow water equation for long waves is expressed in the polar coordination, which is solved through separation of variables. As the topography is axisymmetric, solutions can be written as Fourier-cosine series. Waves over the seamount are expressed using Frobenius series expansion, while the water surface elevation in the outer region is expressed as Fourier-Bessel series, and the final solution is obtained by matching them at the conjunction. The solution can be degenerated into the previous analytic solutions for waves propagation over an axisymmetric pit or a submerged hump by adjusting the topography parameters.

Keywords: Long waves; analytic solution; wave motion; seamount with a pit; wave propagation

1 Introduction

The earthquake in the Sumatra Sea, northern Indonesia on December 26, 2004 triggered a strong tsunami that caused tremendous casualties and property damage in Southeast Asia and South Asian countries (Synolakis and Bernard, 2006). Since then, the study of long-wave (e.g. tsunami wave) propagation in shallow water attracts more attention. Tsunami arrival time and run-up are the most important information for disaster prevention and reduction, but they are highly relevant to the propagation paths that feature with the scattering of submarine topographies (Satake, 1988). The ocean ridges, seamounts and the continental shelf may all act as natural guides for the propagation of long

* Email address for correspondence: jhzheng@hhu.edu.cn

waves (such as tsunami) far away from its source (Titov et al., 2005).

Seamounts are one of the most common geomorphic features of the seabed. To understand the focusing and scattering phenomena of tsunamis or other long waves on the seamount is of practical significance for real-time tsunami prediction and coastal protection. Related to this, a series of research results obtained using different methods have been reported for wave transformation caused by three-dimensional topographies, such as islands or submerge shoals. The earliest study may be traced back to Homma (1950), who resolved a vertical cylindrical islands mounted on a parabolic shoal. The results showed that, for a particular incident wave frequency, the wave amplitude was unusually large on the shoal. Vastano and Reid (1967) validated Homma's results using a finite difference numerical model on a truncated domain. Longuet-Higgins (1967) presented in-depth work on the energy-trapping phenomenon of underwater axisymmetric topography. He considered a case of wave propagation over a submerged circular cylinder and mathematically proved that wave energy cannot be fully captured by a submerged circular sill and certain amount of energy will leak to infinity. As the leaked energy is extremely small for certain specific frequencies, the energy is nearly trapped in the vicinity of the topography. Such a near-trapping phenomenon corresponds to a large response from the topography, which is described as near-resonance. Barnard et al. (1983) conducted experiments to examine possible trapping of surface waves by a submerged circular sill. They observed that resonance is activated at certain locations over the sill and the wave amplitude could be amplified 4 to 5 times. Chamberlain and Porter (1999) adopted the modified mild-slope equation to approximate the scattering and near-trapping of surface waves by axisymmetric submerged circular shoals of variable water depth. Their results proved that, for each mode, near-trapping phenomena may be associated with a set of discrete frequencies and the degree of resonance response to the trapping is closely related to the topography. Energy leakage may also affect the pattern of long-distance wave propagation. The transoceanic tsunami caused by the 2006 Kuril Islands earthquake (M8.3) propagated across the entire Pacific Ocean. Tidal gauge records along the Pacific coast of Japan show that the maximum tsunami wave arrived more than 5 hours later than the primary wave. The simulation results reported by Koshimura et al. (2008) indicated that the possible reason may be due to wave scattering caused by the Emperor seamounts.

For a more complex bottom geometry, Zhu and Zhang (1996) derived analytical solutions for the propagation of long surface waves around a conical island and over a paraboloidal shoal, where the

paraboloid shoal is described as $h(r) = a r^2$ (r is the radial distance and the a is a topography parameter). Lin (2007) presented an analytic solution of the gentle slope equation for wave scattering and trapping around a truncated paraboloid shoal defined as $h(r) = a r^2$ (where r is the radial distance and the a is a topography parameter). Liu and Li (2007) sought an analytical solution for wave scattering by a submerged circular truncated shoal with the bottom geometry being an arbitrary power function $h(r) = ar^m$. Zhu and Harun (2009) further derived an analytic solution of long-wave over a quasi-ideal parabolic shoal defined by the water-depth function $h(r) = ar^2 + h_0$ (where h_0 is the minimum water depth of the hump). Niu and Yu (2011a) and Liu and Xie (2011) generalized the shoal with power function profiles $h(r) = ar^m + h_0$ (m is any positive integer) and presented the analytic solution to explore the impact of the shape, size, height of shoal on the focus position and the maximum wave amplitude.

With the increased dredging activities in recent years, offshore areas tend to leave a lot of dredging pit. The change of the offshore topography will affect the transformation process of waves and result in substantial shoreward salient and associated erosional areas. Therefore, research on wave propagation over dredge pits has received more attention. Bender and Dean (2005) used a step method and numerical method to examine the interaction of linear water waves with two-dimensional trenches and shoals. Suh et al. (2005) derived an analytic solution of the mild slope wave equation for long wave propagation over a bowl-shaped pit located in an otherwise constant depth region, and explored the effects of the pit dimensions on wave scattering. Jung and Suh (2007) further extended their solution to a pit with water depth decreasing in proportion to an integer power of radial distance from the pit center. Niu and Yu (2011b) and Liao et al. (2014) respectively derived analytic solutions of the mild-slope wave equation to describe wave propagation over an idealized axisymmetrical dredge excavation pit composed of a flat bottom and a convex slope.

There are nearly 10,000 seamounts identified in different regions around the world, and many of them have a funnel or bowl shape crater at the top of a cone. The example is Vailulu'u seamount, whose summit includes a 400-m-deep and 2-km-wide crater (Hart et al., 2000). The Brothers Volcano located in the northeastern New Zealand has a large bowl-shape volcanic pit with diameter of 3000m and depth of 500m at the center (Embley et al., 2012). These pits over the top of the seamount must induce different scattering pattern of long waves. Although the scattering phenomena of long waves on seamounts has be widely studied, further research is still deserved to improve our understanding on

wave propagation over seamounts with a pit. This paper will first try to derive an analytic solution for wave propagation over an idealized seamount with a pit. The analytic solution is then compared with existing analytic solutions previously derived for different bottom geometries. The effects of different topography parameters on the wave scattering are also discussed in detail.

2 The Physical Problem under Consideration

The physical problem of our primary interest is shown in Figure 1. We consider long waves scattering over a circular seamount with a circular pit. The origin of the horizontal coordinate system is taken to be the center of the pit, where r is the radial distance from the origin, and θ is the angle measured counterclockwise from the positive x-axis. The water depth in the radial direction varies according to

$$h(r)=\begin{cases} ar^{4/m}-br^{2/m}+h_0 & 0<r\le r_2 \\ h_2 & r>r_2 \end{cases} \tag{1}$$

where a and b are terrain parameters, m is a positive integer, r_1 and r_2 are the radial distances from the center to the pit edge and the island toe respectively, h_0 is the water depth at the pit center, h_1 and h_2 are the water depths along the crest of the ridge and beyond the pit, which can be expressed as

$$h_1=ar_1^{4/m}-br_1^{2/m}+h_0 \tag{2}$$

and

$$h_2=ar_2^{4/m}-br_2^{2/m}+h_0 \tag{3}$$

Based on the linear shallow water equation, the long-wave equation can be written in polar coordinates (r, θ) as follows (Mei et al., 2005):

$$r^2\frac{\partial^2\eta}{\partial r^2}+r\left(1+\frac{r}{h}\frac{\partial h}{\partial r}\right)\frac{\partial\eta}{\partial r}+\frac{1}{h}\frac{\partial h}{\partial\theta}\frac{\partial\eta}{\partial\theta}+\frac{\partial^2\eta}{\partial\theta^2}+\frac{\omega^2r^2}{gh}\eta=0 \tag{4}$$

where $\eta(r,\theta)$ is the water surface elevation, $h(r)$ is the still water depth, ω is the angular frequency, and g is the gravitational acceleration.

3. Analytic solution

3.1 In the inner region with variable depth [0, r_2]

Due to the axisymmetric topography of the seamount, the solution for wave propagation may be expressed as a Fourier-cosine series (Mei et al., 2005)

$$\eta(r,\theta)=\sum_{n=0}^{\infty}R_n(r)\cos n\theta \tag{5}$$

in which the integer n corresponds to nth angular mode and $R_n(r)$ is the corresponding coefficient

varying in the r direction. Substituting Eqs. (1) and (5) into Eq. (4) leads to

$$\frac{d^2R_n}{dr^2}+\frac{\left[(4/m+1)ar^{4/m}-(2/m+1)br^{2/m}+h_0\right]}{r\left(ar^{4/m}-br^{2/m}+h_0\right)}\frac{dR_n}{dr}+\frac{\left[\mu r^2-n^2\left(ar^{4/m}-br^{2/m}+h_0\right)\right]}{r^2\left(ar^{4/m}-br^{2/m}+h_0\right)}R_n=0 \qquad (6)$$

where $\mu=\omega^2/g$。

As the above differential equation will be solved through series solution, its convergence is examined herein. The singularities for Eq. (6) are

(i) $r = 0$;

(ii) All the complex roots of $ar^{4/m} - br^{2/m} + h_0 = 0$, i.e.：

$$r=r_1\left(1\pm\sqrt{\frac{h_1}{h_0-h_1}}\mathrm{i}\right)^{\frac{m}{2}}e^{i\pi ml}$$

where

$$\begin{cases} l=0,1 & m\in \text{odd} \\ l=0 & m\in \text{even} \end{cases}$$

Thus, all roots are located at the circle with radius of

$$|r|=r_1\left(\frac{h_0}{h_0-h_1}\right)^{\frac{m}{4}} \qquad (7)$$

As the terrain parameters a and b can be expressed as

$$\begin{aligned} a&=\left(h_0-h_1\right)/r_1^{4/m} \\ b&=2ar_1^{2/m} \end{aligned} \qquad (8)$$

Thus, the radius r_2 can be derived as

$$r_2=\left[\frac{b\pm\sqrt{b^2-4a(h_0-h_2)}}{2a}\right]^{\frac{m}{2}}=r_1\left[1\pm\sqrt{\frac{(h_2-h_1)}{(h_0-h_1)}}\right]^{\frac{m}{2}} \qquad (9)$$

As the radial distances from the center to the island toe r_2 larger than the radial distances from the center to the pit edge r_1, the minus sign in the above equation should be deleted, that is

$$r_2=r_1\left[1+\sqrt{\frac{(h_2-h_1)}{(h_0-h_1)}}\right]^{\frac{m}{2}}\geq r_1\left[1+\frac{(h_2-h_1)}{(h_0-h_1)}\right]^{\frac{m}{4}}=r_1\left[\frac{h_0+\left(h_2-2h_1\right)}{h_0-h_1}\right]^{\frac{m}{4}} \qquad (10)$$

It implies that all singular points are located into the complex disk $|r| < r_2$ if h_2 is greater than $2h_1$. As shown in Figure 2, there are four complex roots to $ar^{4/m} - br^{2/m} + h_0 = 0$ for $m = 1$ and two complex roots for $m = 4$, and all of them are in convergent domain. Then, it is impossible to determine convergent solutions at these singular points.

In order to derive the solution considering the case $h_2 \geq 2h_1$, the following transformation is used:

$$\rho = r^{2/m} \tag{11}$$

$$R_n(r) = \tilde{R}_n(\rho) = \tilde{R}_n\left(r^{2/m}\right) \tag{12}$$

and now Eq. (6) can be rewritten as：

$$\rho^2 \frac{d^2\tilde{R}_n}{d\rho^2} + \rho\left(\frac{3a\rho^2 - 2b\rho + h_0}{a\rho^2 - b\rho + h_0}\right)\frac{d\tilde{R}_n}{d\rho} + \left[\frac{m^2\mu\rho^m}{4\left(a\rho^2 - b\rho + h_0\right)} - \frac{n^2m^2}{4}\right]\tilde{R}_n = 0 \tag{13}$$

Using the above transformation, the inner region $0 \leq r \leq r_2$ has been mapped on to $0 \leq \rho \leq \rho_2$, where $\rho_2 = r_2^{2/m}$. There are three singular points to Eq. (13), i.e., $\rho = 0$ and two complex roots of $a\rho^2 - b\rho + h_0 = 0$, as shown in Figure 3.

The whole inner region $[0, \rho_2]$ can be split into $I_1 = [0, \rho_1]$ and $I_2 = [\rho_1, \rho_2]$, where $\rho_1 = r_1^{2/m}$. So, the solutions for Eq. (13) in these two sub-regions may be expanded at points $\rho = 0$ and $\rho = \xi = (\rho_1+\rho_2)/2$, i.e., the solutions are expanded into a Frobenius series at $\rho = 0$ in I_1 and a Taylor series at $\rho = \xi$ in I_2. The convergence of the solutions in each sub-region is therefore guaranteed.

Region $I_1[0, \rho_1]$:

According to the Frobenius theory (Spiegel., 1967), the solution of Eq. (13) can be expressed as

$$\tilde{R}_n(\rho) = \sum_{j=0}^{\infty} \alpha_{n,j}\rho^{j+c} \tag{14}$$

where $\alpha_{n,j}$ is a constant to be determined.

Inserting Eq. (14) into Eq. (13) yields：

$$\begin{aligned} &\sum_{j=0}^{\infty} a\left[4(j+c)(j+c+2) - n^2m^2\right]\alpha_{n,j}\rho^{j+c+2} - \sum_{j=0}^{\infty} b\left[4(j+c)(j+c+1) - n^2m^2\right]\alpha_{n,j}\rho^{j+c+1} \\ &+ \sum_{j=0}^{\infty} h_0\left[4(j+c)^2 - n^2m^2\right]a_{n,j}\rho^{j+c} + \sum_{j=0}^{\infty} m^2\mu\alpha_{n,j}\rho^{j+c+m} = 0 \end{aligned} \tag{15}$$

The parameter c can be obtained by setting $j = 0$ for the above equation, giving $c = \pm nm/2$.

Two special solutions of $\tilde{R}_n$ denoted by $\tilde{R}_{1,n}$ and $\tilde{R}_{2,n}$ may be written in the following form (Spiegel., 1967)：

$$\tilde{R}_{1,n}(\rho) = \sum_{j=0}^{\infty} \alpha_{n,j}\rho^{j+\frac{nm}{2}} \tag{16}$$

$$\tilde{R}_{2,n}(\rho) = \tilde{R}_{1,n}\ln\rho + \sum_{j=0}^{\infty} \beta_{n,j}\rho^{j-\frac{nm}{2}} \tag{17}$$

As $\tilde{R}_{2,n}$ is singular at $\rho = 0$ and should be discarded. The solution in Eq. (14) can be expressed as

$$\tilde{R}_n(\rho) = A_n \sum_{j=0}^{\infty} \alpha_{n,j} \rho^{j+\frac{nm}{2}} \tag{18}$$

Thus, R_n, the solution in Eq. (6), can be written as

$$R_n(r) = A_n \sum_{j=0}^{\infty} \alpha_{n,j} (r)^{n+\frac{2j}{m}} \tag{19}$$

When m =1, Eq. (15) becomes

$$\alpha_{n,j} = \begin{cases} 1 & (j=0) \\ \dfrac{(2bn-\mu)\alpha_{n,0}}{4h_0(n+1)} & (j=1) \\ \dfrac{-a\left(4j^2+4jn-8j-4n\right)\alpha_{n,j-2} + b\left(4j^2+4jn-4j-2n\right)\alpha_{n,j-1} - \mu\alpha_{n,j-1}}{4h_0\left(j^2+jn\right)} & (j \geq 2) \end{cases} \tag{20}$$

When m = 2, Eq. (15) gives

$$\alpha_{n,j} = \begin{cases} 1 & (j=0) \\ \dfrac{bn\alpha_{n,0}}{h_0(2n+1)} & (j=1) \\ \dfrac{-\left[a\left(j^2+2jn-2j-2n\right)+\mu\right]\alpha_{n,j-2} + b\left(j^2+2jn-j-n\right)\alpha_{n,j-1}}{h_0\left(j^2+2jn\right)} & (j \geq 2) \end{cases} \tag{21}$$

When m > 2, we have

$$\alpha_{n,j} = \begin{cases} 1 & (j=0) \\ \dfrac{nmb\alpha_{n,0}}{2h_0\left(1+nm\right)} & (j=1) \\ \dfrac{-a\left(4j^2+4jnm-8j-4nm\right)\alpha_{n,j-2} + b\left(4j^2+4jnm-4j-2nm\right)\alpha_{n,j-1}}{4h_0\left(j^2+jnm\right)} & (2 \leq j < m) \\ \dfrac{-a\left(4j^2+4jnm-8j-4nm\right)\alpha_{n,j-2} + b\left(4j^2+4jnm-4j-2nm\right)\alpha_{n,j-1} - \mu p^2 \alpha_{n,j-m}}{4h_0\left(j^2+jnm\right)} & (j \geq m) \end{cases} \tag{22}$$

Finally, the water surface elevation in region [0, r_1] is obtained：

$$\eta_1(r,\theta) = \sum_{n=0}^{\infty} R_n(r)\cos n\theta = \sum_{n=0}^{\infty} A_n T_n(r)\cos n\theta \tag{23}$$

where

$$T_n(r)=\sum_{j=0}^{\infty}\alpha_{n,j}r^{\frac{2j}{m}+n} \tag{24}$$

Region I_2 [ρ_1, ρ_2]:

As there is no singularity for Eq. (13) in the complex field $|\rho - \xi| \le \xi - \rho_1$, its solution may be expanded into a Taylor series at ξ as follows (Spiegel., 1967)

$$\tilde{R}_n(\rho)=\sum_{j=0}^{\infty}u_{n,j}(\rho-\xi)^j \tag{25}$$

For the sake of convenience, Eq. (13) is rewritten in the form

$$\tilde{R}_n''+\tilde{P}(\rho)\tilde{R}_n'+\tilde{Q}(\rho)\tilde{R}_n=0 \tag{26}$$

in which

$$\tilde{P}(\rho)=\frac{3a\rho^2-2b\rho^2+h_0}{\rho\left(a\rho^2-b\rho+h_0\right)} \tag{27}$$

$$\tilde{Q}(\rho)=\frac{m^2\mu\rho^m-n^2m^2\left(a\rho^2-b\rho+h_0\right)}{4\rho^2\left(a\rho^2-b\rho+h_0\right)} \tag{28}$$

$\tilde{P}(\rho)$ and $\tilde{Q}(\rho)$ are also expanded into a Taylor series at ξ as:

$$\tilde{P}(\rho)=\sum_{l=0}^{\infty}\frac{\tilde{P}^{(l)}(\rho)\big|_{\rho=\xi}}{l!}(\rho-\xi)^l \tag{29}$$

$$\tilde{Q}(\rho)=\sum_{l=0}^{\infty}\frac{\tilde{Q}^{(l)}(\rho)\big|_{\rho=\xi}}{l!}(\rho-\xi)^l \tag{30}$$

Substitution of Eqs. (25), (29) and (30) into Eq. (26) leads to

$$\begin{aligned}\tilde{R}_n(\rho)&=\beta_{1,n}U_n(\rho)+\beta_{2,n}V_n(\rho)\\&=\beta_{1,n}\sum_{j=0}^{\infty}u_{n,j}(\rho-\xi)^j+\beta_{2,n}\sum_{j=0}^{\infty}v_{n,j}(\rho-\xi)^j\\&=\beta_{1,n}\sum_{j=0}^{\infty}u_{n,j}\left(r^{2/m}-\xi\right)^j+\beta_{2,n}\sum_{j=0}^{\infty}v_{n,j}\left(r^{2/m}-\xi\right)^j\end{aligned} \tag{31}$$

where $\beta_{1,n}$ and $\beta_{2,n}$ are the coefficients determined by the matching conditions, and

$$\begin{aligned}&u_{n,0}=1\\&u_{n,1}=0\\&u_{n,j}=-\frac{\sum_{i=0}^{j-2}\left[(j-i+1)\frac{\tilde{P}^{(i)}(\xi)}{i!}u_{n,j-i-1}+\frac{\tilde{Q}^{(i)}(\xi)}{i!}u_{n,j-i-2}\right]}{j(j-1)}\qquad j=2,3,\cdots,\end{aligned} \tag{32}$$

$$
\begin{aligned}
&v_{n,0} = 0 \\
&v_{n,1} = 1 \\
&v_{n,j} = -\frac{\sum_{i=0}^{j-2}\left[(j-i+1)\frac{\tilde{P}^{(i)}(\xi)}{i!}v_{n,j-i-1} + \frac{\tilde{Q}^{(i)}(\xi)}{i!}v_{n,j-i-2}\right]}{j(j-1)} \qquad j = 2,3,\cdots,
\end{aligned} \tag{33}
$$

finally, the water surface elevation in the region $[r_1, r_2]$ is obtained and expressed as：

$$
\eta_2(r,\theta) = \sum_{n=0}^{\infty} R_n(r)\cos n\theta = \sum_{n=0}^{\infty}\left[\beta_{1,n}U_n(r) + \beta_{2,n}V_n(r)\right]\cos n\theta \tag{34}
$$

in which

$$
\begin{aligned}
U_n(r) &= \sum_{j=0}^{\infty} u_{n,j}\left(r^{2/m} - \xi\right)^j \\
V_n(r) &= \sum_{j=0}^{\infty} v_{n,j}\left(r^{2/m} - \xi\right)^j
\end{aligned} \tag{35}
$$

3.2 In the outer region with a constant depth (r_2, ∞)

In this region, there are incident waves from the open sea $\eta_I(r, \theta)$ and scattered waves by the seamount $\eta_S(r, \theta)$. The water surface elevation $\eta(r, \theta)$ may be expressed as

$$
\eta(r,\theta) = \eta_I(r,\theta) + \eta_S(r,\theta) \tag{36}
$$

The incident wave may be assumed as a linear sinusoidal wave propagating in the positive x direction, which can be expressed using a Fourier-cosine series as (Mei et al., 2005),

$$
\eta_I = A_I e^{ik_2 x} = A_I \sum_{n=0}^{\infty} \mathrm{i}^n \varepsilon_n \mathrm{J}_n(k_2 r)\cos n\theta \tag{37}
$$

where A_I is the incident wave amplitude, $k_2 = \omega/(gh_2)^{1/2}$ is the corresponding wavenumber, J_n is the nth order Bessel function of the first kind and ε_n is the Jacobi symbol defined by

$$
\varepsilon_n = \begin{cases} 1, & n = 0 \\ 2, & n \geq 1 \end{cases} \tag{38}
$$

The scattered wave may be expressed as (Wang et al., 2011)

$$
\eta_S(r,\theta) = \sum_{n=0}^{\infty} D_n \mathrm{H}_n(kr)\cos n\theta \tag{39}
$$

where D_n is the complex constant to be determined, H_n is the nth order Hankel function of the first kind. The water surface elevation in the outer region can finally be obtained:

$$
\eta_3(r,\theta) = A_I \sum_{n=0}^{\infty} \mathrm{i}^n \varepsilon_n \mathrm{J}_n(k_2 r)\cos n\theta + \sum_{n=0}^{\infty} D_n \mathrm{H}_n(k_2 r)\cos n\theta \tag{40}
$$

3.3 Matching Conditions

The domain concerned is divided into three regions: the outer region with constant water depth ($r \geq r_2$)

and two inner regions with variable water ($0 \le r < r_1$ and $r_1 \le r < r_2$). The strategy here is to find the general solutions in each region and then match them at the boundaries to obtain the overall solution for the full domain. The water surface and its derivative are continuous at $r = r_1$ and $r = r_2$, which requires

$$\eta_1\big|_{r=r_1} = \eta_2\big|_{r=r_1} \tag{41}$$

$$\eta_2\big|_{r=r_2} = \eta_3\big|_{r=r_2} \tag{42}$$

$$\left.\frac{\partial \eta_1}{\partial r}\right|_{r=r_1} = \left.\frac{\partial \eta_2}{\partial r}\right|_{r=r_1} \tag{43}$$

$$\left.\frac{\partial \eta_2}{\partial r}\right|_{r=r_2} = \left.\frac{\partial \eta_3}{\partial r}\right|_{r=r_2} \tag{44}$$

Using the expressions (23), (34) and (40), the matching relationships as defined in (41) - (44) give

$$A_n T_n(r_1) = \beta_{1,n} U_n(r_1) + \beta_{2,n} V_n(r_1) \tag{45}$$

$$A_1 \mathrm{i}^n \varepsilon_n \mathrm{J}_n(k_2 r_2) + D_n \mathrm{H}_n(k_2 r_2) = \beta_{1,n} U_n(r_2) + \beta_{2,n} V_n(r_2) \tag{46}$$

$$A_n T_n'(r_1) = \beta_{1,n} U_n'(r_1) + \beta_{2,n} V_n'(r_1) \tag{47}$$

$$k_2 \left(A_1 \mathrm{i}^n \varepsilon_n \mathrm{J}_n'(k_2 r_2) + D_n \mathrm{H}_n'(k_2 r_2) \right) = \beta_{1,n} U_n'(r_2) + \beta_{2,n} V_n'(r_2) \tag{48}$$

All coefficients can be determined by solving Eqs. (45)-(48)：

$$\beta_{1,n} = \frac{k_2 A_1 \mathrm{i}^n \varepsilon_n \left[-\mathrm{J}_n'(k_2 r_2) \cdot \mathrm{H}_n(k_2 r_2) + \mathrm{J}_n(k_2 r_2) \cdot \mathrm{H}_n'(k_2 r_2) \right]}{\left[k_2 U_n(r_2) \mathrm{H}_n'(k_2 r_2) - U_n'(r_2) \cdot \mathrm{H}_n(k_2 r_2) \right] + \left[k_2 V_n(r_2) \mathrm{H}_n'(k_2 r_2) - V_n'(r_2) \cdot \mathrm{H}_n(k_2 r_2) \right] \chi} \tag{49}$$

$$\beta_{2,n} = \chi \beta_{1,n} \tag{50}$$

$$A_n = \frac{\left[U_n(r_1) + \chi V_n(r_1) \right] \beta_{1,n}}{T_n(r_1)} \tag{51}$$

$$D_n = \frac{U_n(r_2) \beta_{1,n} + V_n(r_2) \beta_{2,n} - A_1 \mathrm{i}^n \varepsilon_n \mathrm{J}_n(k_2 r_2)}{\mathrm{H}_n(k_2 r_2)} \tag{52}$$

where

$$\chi = \frac{U_n'(r_1) \cdot T_n(r_1) - U_n(r_1) \cdot T_n'(r_1)}{V_n(r_1) T_n'(r_1) - V_n'(r_1) \cdot T_n(r_1)} \tag{53}$$

The analytic solution of the free surface η involves infinite series, and these series require proper

truncation for the calculus. The truncation error is defined as $er = (\eta_N - \eta_{N-1})/\eta_N$, and the summation process is stopped when $er < 10^{-6}$. Our calculation results show that $N > 70$ is large enough to guarantee convergence to the truncation error.

4 Comparison with existing solution

As shown in Figure 1, when r_2 approaches to r_1, h_2 will become close to h_1; meanwhile, the ridge surrounding the seamount will disappear and the topography will degenerate into a pit with a uniform water depth. So, the analytic solution derived in the previous section can also be suitable to describe wave refraction over a dredge excavation pit. On the other hand, when r_1 approaches to zero, h_0 will become close to h_1; the pit mounded on the seamount disappears and the topography degenerates into a submerged hump with a uniform water depth if $h_0 < h_2$. Therefore, the analytic solution can also be used to describe wave propagation over a submerged hump.

Jung and Suh (2007) derived an analytic solution to the mild slope equation for wave propagation over an axisymmetric pit and presented results for a case with $h_0 = 6.4$ m, $h_1 = 3.2$ m, $k_1h_1 = 0.167$ and $r_1 = \pi/k_1$. Adopting the same geometric parameters and wave conditions, comparisons are made between the current analytical solution with $r_2 = 1.01r_1$ and $m = 1$ and the results of Jung and Suh (2007) for $\alpha = 1$. The relative wave amplitude along the x-axis is shown in Figure 4. Overall good agreement is observed between the two solutions. Slight discrepancy appears due to the difference of the current topography to that of Jung and Suh (2007).

Niu and Yu (2011a) derived an analytic solution for long wave refraction by a submerged circular hump, and presented results for $h_1 = 3.2$ m, $h_2 = 4.8$ m, $k_2h_2 = 0.3$ and $r_2 = \pi/k_2$. The current solution with $h_0 = 1.01h_1$, $r_1 = 0.5$ m and $m = 4$ is compared with results of Niu and Yu (2011a) for $\alpha = 1$. The overall good agreement is obtained between the two sets of solutions as shown in Figure 5.

5 Results and Discussion

5.1 Effects of seamount scale

In this subsection, the newly derived analytic solution is applied to investigate the effects of the seamount scale on wave scattering. The radius of the seamount r_2 is varied, while r_1 is specified to maintain the ration to r_2 so that $r_1 = 2r_2/3$. The other parameters are chosen to be $h_0 = 7.3$ m, $h_1 = 3.2$ m, $m = 1$ and $k_2h_2 = 0.3$. The constant depth beyond the pit h_2 can be obtained by solving Eqs.(3) and (8), i.e., $h_2 = (h_0 - h_1)(r_2/r_1)^{4/m} - 2(h_0 - h_1)(r_2/r_1)^{2/m} + h_0$. The distributions of the relative wave

amplitude for $k_2r_2 = 0.3\ \pi$, $k_2r_2 = 0.5\ \pi$, $k_2r_2 = 1.0\ \pi$, $k_2r_2 = 1.5\ \pi$, $k_2r_2 = 2.0\ \pi$ and $k_2r_2 = 2.5\ \pi$ are shown in Figure 6, where the corresponding terrain parameters a and b can be obtained by Eq.(8).

The larger radius of the seamount causes the more complex distribution of wave-amplitude, which implies the more intensive scattering effect. When the radius of the seamount is smaller than the wavelength, the seamount cannot exert an obvious impact on the waves. Waves can directly propagate over the small seamount and the wave amplitude is larger in the pit than other areas. The scattering effect is enhanced with the increase of the seamount radius. Partial standing waves in front of the pit increase with the radius. More wave energy is scattered laterally due to refraction and diffraction for larger seamounts, and the scattering wave pattern around becomes more complicated.

Due to the clear refraction and reflection effects of the pit for larger seamounts, the minimal amplitude appears near the center, although its exact position varies with the radius. Figure 7 shows the relative maximum wave amplitude $\lambda = \eta_{max}/A_1$ and its corresponding location for different seamount radius r_2. The relative maximum wave amplitude λ increases with the seamount radius, and its corresponding location first shifts backwards as the seamount radius increases until $k_2r_2 > 1.35$ and then rounds the wing ridge axisymmetrically.

5.2 Effects of pit depth

In this subsection, the influence of pit depth h_0 on wave scattering is examined. As shown in Figure 8(a), the geometric parameters are set to $h_1 = 3.2$ m, $h_2 = 5.4$ m, $k_2h_2 = 0.167$, $r_1 = \pi/k_2$ and $r_2 = 2r_1$; the central depth of the pit, i.e. h_0, takes the values of 3.45 m, 5.40 m and 9.60 m respectively, with the corresponding value of m varying between 1, 2 and 3.

Figure 9 shows the relative wave amplitudes along the x-axis and y-axis for different pit depths. With the increase of the depth of dip, wave-amplitude in the pit and at lee side of ridge along the x-axis increases, but it decreases at the wing ridge on both sides along the y-axis. The corresponding wave amplitude distributions for different pit depths are shown in Figure 10. There is a reduction of wave heights in the shadow zone for the deeper pit, and the location of the smallest wave height in the shadow zone is shifted backwards.

5.3 Effects of ridge crest depth

In this subsection, the effect of the ridge crest depth on wave scattering is discussed. The parameters are set to $h_0 = h_2 = 5.40$ m, $k_2h_2 = 0.167$, $r_1 = \pi/k_2$, $m = 1$ and $r_2 = 2^{m/2}r_1$ while the crest depth takes the following values: $h_1 = 3.6$m, 3.0m, 2.4m, 1.8m and 1.2 m, leading to a steeper seamount, as shown in

Figure 8.b. Figure 11 shows the variation of the relative amplitude along the x-axis and y-axis for different crest depth h_1. The smaller crest depth indicates the steeper topography and the enhancement of the waves around the seamount becomes evident. As the crest depth decreases, partial standing waves in front of the seamount increase due to wave reflection. The amplitude at the ridge of the lee side together with the wing ridge on both sides is enhanced dramatically due to wave refraction.

Figure 12 shows the overall distribution of the relative wave amplitude for h_1 =1.2 m, 2.4 m and 3.6 m. Only the waves behind the pit are evidently enhanced for the flat seamount with larger crest depth (see Figure 12.a and b). As the scattering effect becomes evident for the steep topography, the wave pattern over the seamount with h_1 =1.2 m clearly becomes more complicated (see Figure 12.c). Partial standing waves become evident in front of the pit. The waves along the pit crest are also enhanced dramatically in addition to the evident lateral scattered waves.

6 Conclusions

This paper presents an analytic solution for long wave propagation over a submarine seamount with a pit, with the water depth of the axisymmetric seamount expressed by a trinomial function in the radial direction. The linear long wave equation is solved by series solutions. The topographic domain is divided into two sub-regions to avoid the existence of the singular points. Frobenius and Taylor series expansions are used to solve the shallow water equation in the two sub-regions, respectively. The final solution is obtained by matching the analytic water surface and its derivative at the boundaries between the sub-regions.

As the present solution can be used to approximate the water wave propagation over a pit or hump on the uniform water depth, it is compared with the solution for a submerged hump reported by Niu and Yu (2011a) and the solution for an axisymmetric pit by Jung and Suh (2007). The influence of the topographic parameters of the seamount on wave scattering is investigated in detail using the analytical solution. The scattering effect is found to be enhanced with the increase of the seamount radius and the decrease of the pit and ridge crest depth.

7 Acknowledgements

The presented research was supported by the National Natural Science Foundation of China (NO.: 51579090), the National Science Fund for Distinguished Young Scholars (NO.: 51425901) and Innovation Project of Colleges and Universities in JiangSu Province (NO.: 2015B41814).

References

Barnard, B.J.S., Pritchard, W.G., Provis, D.G., 1983. Experiments on wave trapping by a submerged cylindrical island. Geophysical & Astrophysical Fluid Dynamics 24 (24), 23-48.

Bender, C.J., Dean, R.G., 2005. Wave transformation by axisymmetric three-dimensional bathymetric anomalies with gradual transitions in depth. Coastal Engineering 52 (4), 331-351.

Chamberlain, P.G., Porter, D., 1999. Scattering and near-trapping of water waves by axisymmetric topography. Journal of Fluid Mechanics 388 (388), 335-354.

Embley, R.W., de Ronde, C.E.J., Merle, S.G., Davy, B., Tontini, F.C., 2012. Detailed Morphology and Structure of an Active Submarine Arc Caldera: Brothers Volcano, Kermadec Arc. Economic Geology 107 (8), 1557-1570.

Hart, S.R., Staudigel, H., Koppers, A.A.P., Blusztajn, J., Baker, E.T., Workman, R., Jackson, M., Hauri, E., Kurz, M., Sims, K., Fornari, D., Saal, A., Lyons, S., 2000. Vailulu'u undersea volcano: the New Samoa. Geochemistry, Geophysics, Geosystems - G3 1, Citation 2000GC0000108.

Homma, S., 1950. On the behavior of seismic sea waves around circular island. Geophysics Magazine 21 (3), 199-208.

Jung, T.-H., Suh, K.-D., 2007. An analytic solution to the mild slope equation for waves propagating over an axi-symmetric pit. Coastal Engineering 54 (12), 865-877.

Koshimura, S., Hayashi, Y., Munemoto, K., Imamura, F., 2008. Effect of the Emperor seamounts on trans-oceanic propagation of the 2006 Kuril Island earthquake tsunami. Geophysical Research Letters 35 (2), L02611.

Liao, B., Cao, D.-Q., Liu, H.-W., 2014. Wave transformation by a dredge excavation pit for waves from shallow water to deep water. Ocean Engineering 76, 136-143.

Lin, P.Z., 2007. Scattering and trapping of wave energy by a submerged truncated paraboloidal shoal. Journal of Waterway Port Coastal & Ocean Engineering 133 (2), 94-103.

Liu, H.W., Li, Y.B., 2007. An analytical solution for long-wave scattering by a submerged circular truncated shoal. Journal of Engineering Mathematics 57 (2), 133-144.

Liu, H.W., Xie, J.J., 2011. Discussion of “Analytic solution of long wave propagation over a submerged hump” by Niu and Yu (2011). Coastal Engineering 58 (9), 948-952.

Longuet-Higgins, M.S., 1967. On the trapping of wave energy round islands. Journal of Fluid Mechanics 29 (4), 781-821.

Mei, C.C., Stiassnie, M., Yue, D.K.-P., 2005. Theory and Applications of Ocean Surface Waves. World

Scientific, Singapore.

Niu, X., Yu, X., 2011a. Analytic solution of long wave propagation over a submerged hump. Coastal Engineering 58 (2), 143-150.

Niu, X., Yu, X., 2011b. Analytical study on long wave refraction over a dredge excavation pit. Wave Motion 48 (3), 259-267.

Satake, K., 1988. Effects of bathymetry on tsunami propagation: Application of ray tracing to tsunamis. Pure and Applied Geophysics 126 (1), 27-36.

Spiegel., M.R., 1967. Applied differential equations, 2nd edition ed. New Jersey, Prentice-Hall.

Suh, K.-D., Jung, T.-H., Haller, M.C., 2005. Long waves propagating over a circular bowl pit. Wave Motion 42 (2), 143-154.

Synolakis, C.E., Bernard, E.N., 2006. Tsunami science before and beyond Boxing Day 2004. Philosophical Transactions of the Royal Society A: Mathematical, Physical and Engineering Sciences 364 (1845), 2231-2265.

Titov, V., Rabinovich, A.B., Mofjeld, H.O., Thomson, R.E., González, F.I., 2005. The Global Reach of the 26 December 2004 Sumatra Tsunami. Science 309 (5743), 2045-2048.

Vastano, A.C., Reid, R.O., 1967. Tsunami Response for Islands: Verification of a Numerical Procedure.

Wang, G., Dong, G.-H., Perlin, M., Ma, X.-Z., Ma, Y.-X., 2011. An analytic investigation of oscillations within a harbor of constant slope. Ocean Engineering 38, 479-486.

Zhu, S.-P., Harun, F.N., 2009. An analytical solution for long wave refraction over a circular hump. Journal of Applied Mathematics and Computing 30 (1), 315-333.

Zhu, S., Zhang, Y., 1996. Scattering of long waves around a circular island mounted on a conical shoal. Wave Motion 23 (4), 353-362.

Figure captains

Figure 1 Definition sketch of the seamount with a pit.

Figure 2 Singlarities to the Eq.(4)

Figure 3 Singularities to the Eq.(7), expansion points and convergent regions

Figure 4 Comparison between the present analytic solution and results of Jung and Suh (2007)

Figure 5 Comparison between the present analytic solution and results of Niu and Yu (2011a)

Figure 6 The distributions of the relative wave amplitude for seamounts with different radial distance r_2.

Figure 7 Position and amplitude of the maximum focusing points corresponding to different seamounts.

Figure 8 (a) Bottom topography corresponding to different pit depth of h_0, (b) Bottom topography corresponding to different depth of h_1. The corresponding terrain parameters a and b can be obtained by Eq.(8), respectively.

Figure 9 Relative wave amplitude along central axis for different pit depths: along (a) x-axis; (b) y-axis.

Figure 10 The distributions of the relative wave amplitude for different pit depths.

Figure 11 Relative wave amplitude along central axis for different ridge crest depth: along (a) x-axis; (b) y-axis

Figure 12 The distributions of the relative wave amplitude for different ridge crest depth.

Figure

Figure 1

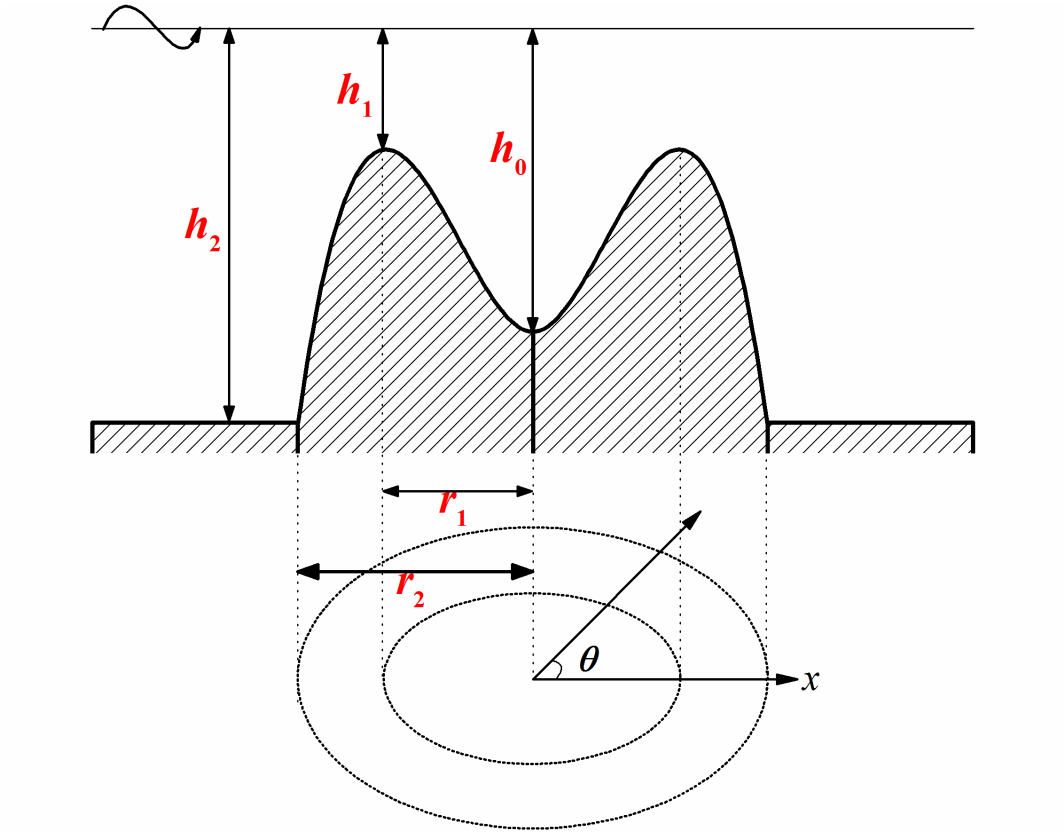

Figure 2

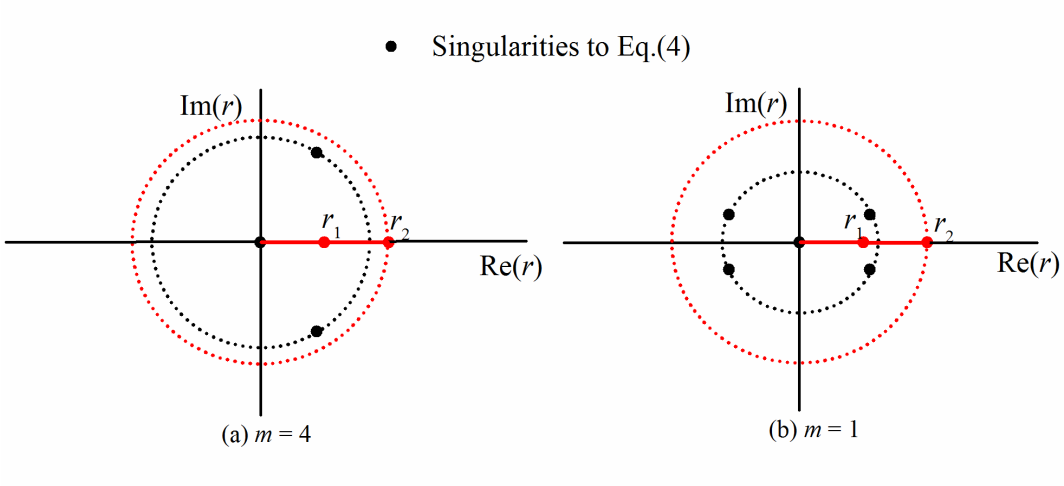

Figure 3

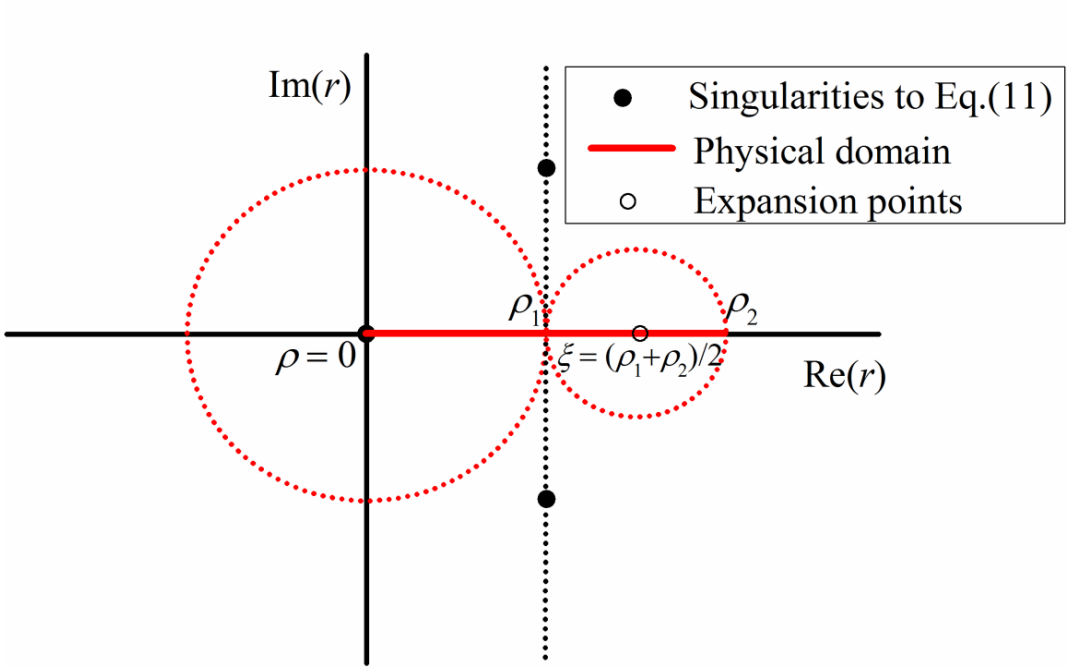
Im(r)
Re(r)
Singularities to Eq.(11)
Physical domain
Expansion points
ρ = 0
ρ1
ρ2
ξ = (ρ1+ρ2)/2

Figure 4

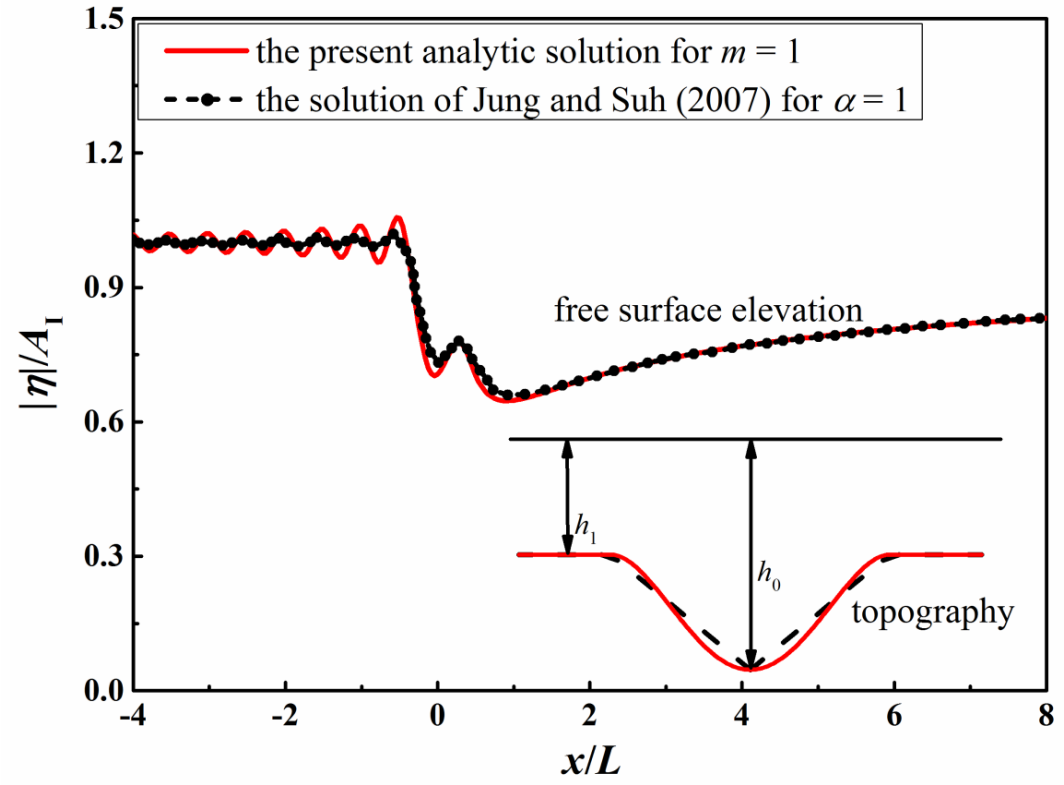
the present analytic solution for $m = 1$
the solution of Jung and Suh (2007) for $\alpha = 1$
free surface elevation
h_1
h_0
topography
$|\eta|/A_I$
x/L
1.5
1.2
0.9
0.6
0.3
0.0
-4
-2
0
2
4
6
8

Figure 5

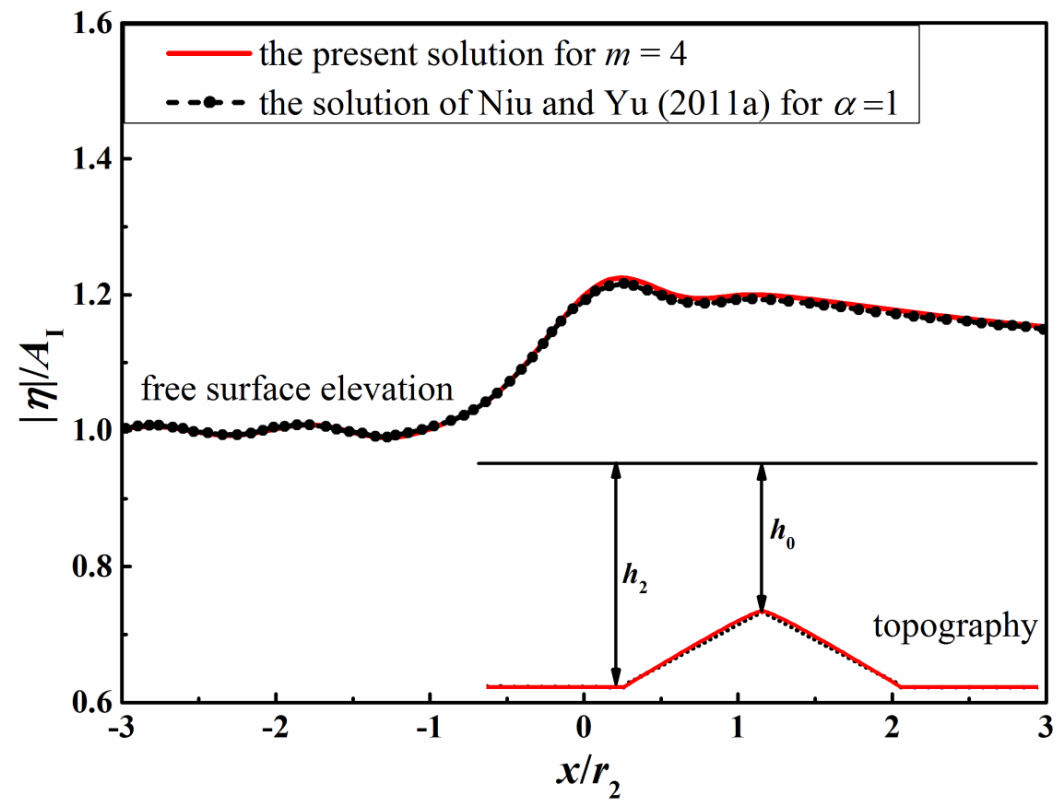
the present solution for $m = 4$
the solution of Niu and Yu (2011a) for $\alpha = 1$
free surface elevation
topography
h_0
h_2
$|\eta|/A_1$
x/r_2
1.6
1.4
1.2
1.0
0.8
0.6
-3
-2
-1
0
1
2
3

Figure 6

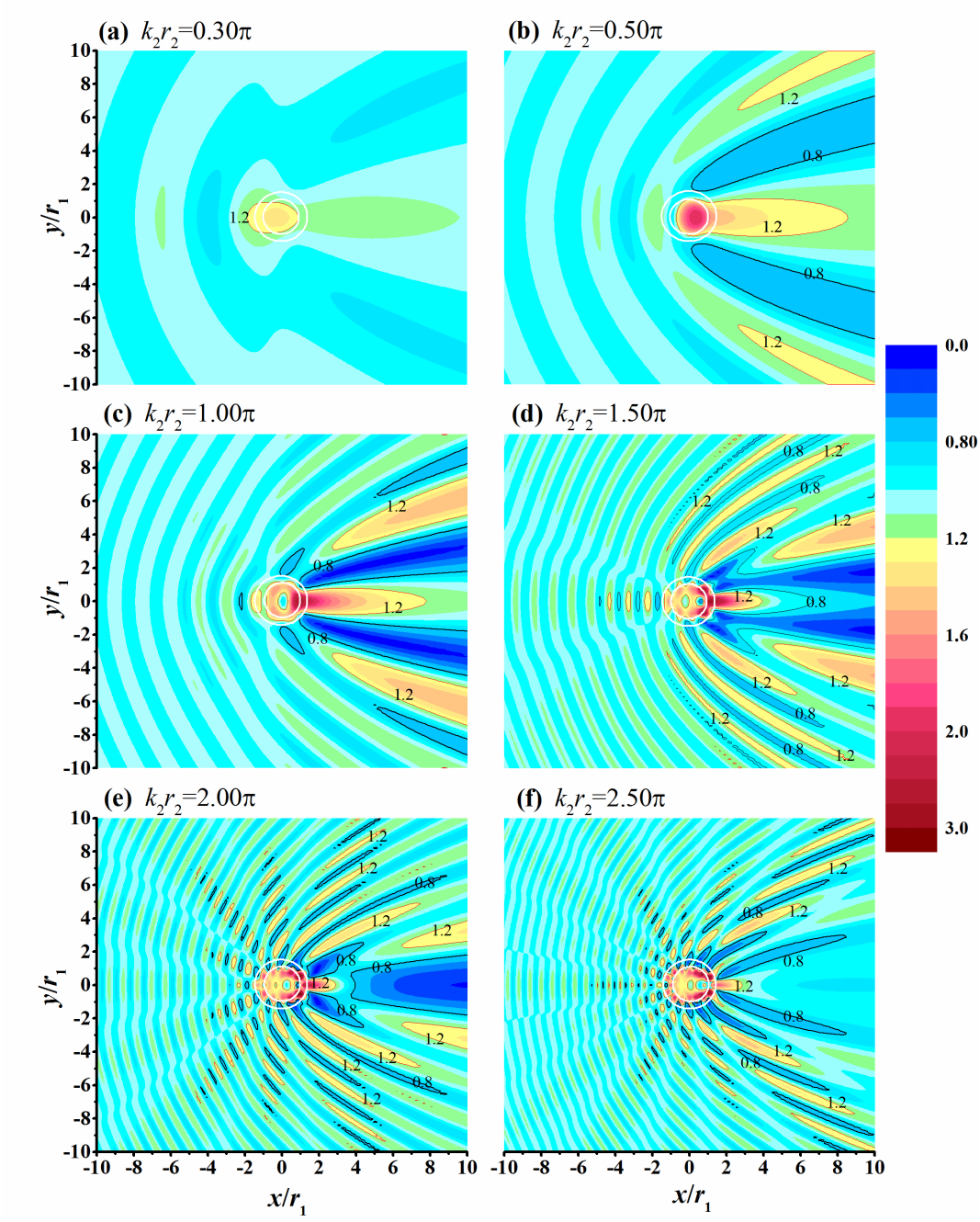
(a) k_2r_2=0.30π
(b) k_2r_2=0.50π
(c) k_2r_2=1.00π
(d) k_2r_2=1.50π
(e) k_2r_2=2.00π
(f) k_2r_2=2.50π
y/r_1
x/r_1
0.0
0.80
1.2
1.6
2.0
3.0

Figure 7

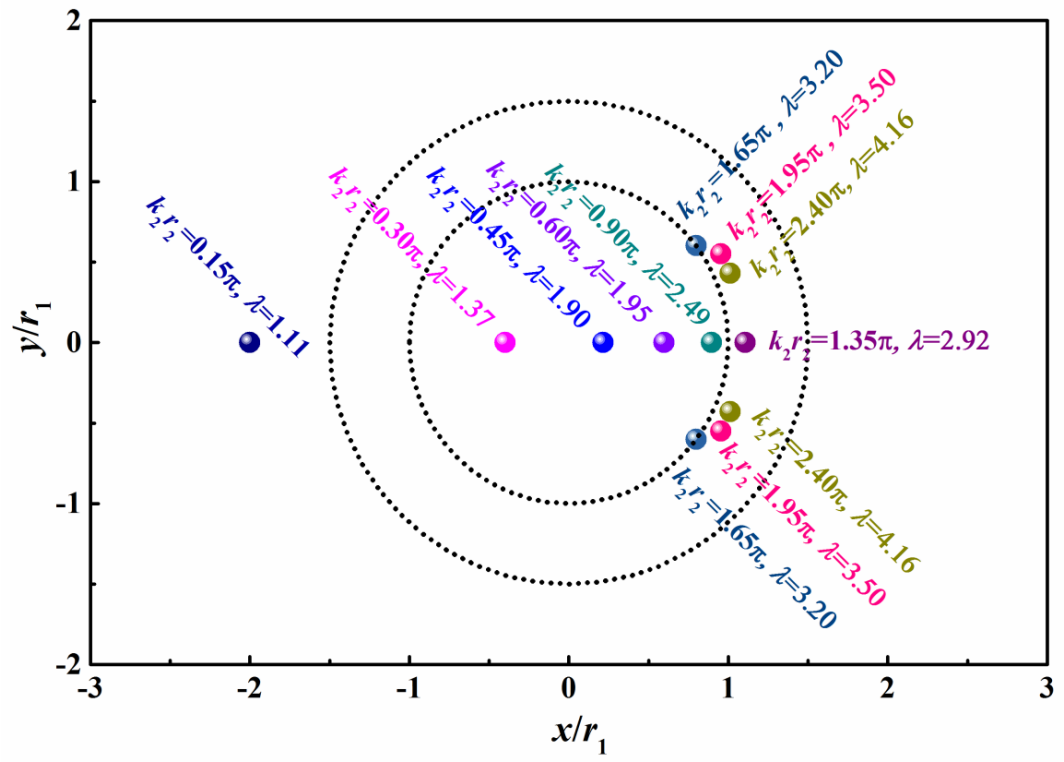
2
1
0
-1
-2
-3
-2
-1
0
1
2
3
y/r1
x/r1
k2r2=0.15π, λ=1.11
k2r2=0.30π, λ=1.37
k2r2=0.45π, λ=1.90
k2r2=0.60π, λ=1.95
k2r2=0.90π, λ=2.49
k2r2=1.35π, λ=2.92
k2r2=1.65π , λ=3.20
k2r2=1.95π , λ=3.50
k2r2=2.40π, λ=4.16
k2r2=2.40π, λ=4.16
k2r2=1.95π, λ=3.50
k2r2=1.65π, λ=3.20

Figure 8

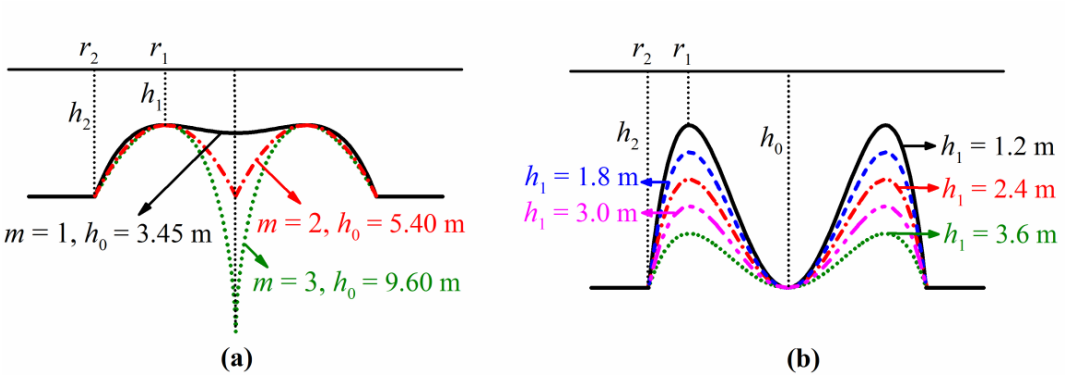
r_2
r_1
h_2
h_1
$m = 1$, $h_0 = 3.45$ m
$m = 2$, $h_0 = 5.40$ m
$m = 3$, $h_0 = 9.60$ m
(a)
r_2
r_1
h_2
h_0
$h_1 = 1.8$ m
$h_1 = 3.0$ m
$h_1 = 1.2$ m
$h_1 = 2.4$ m
$h_1 = 3.6$ m
(b)

Figure 9

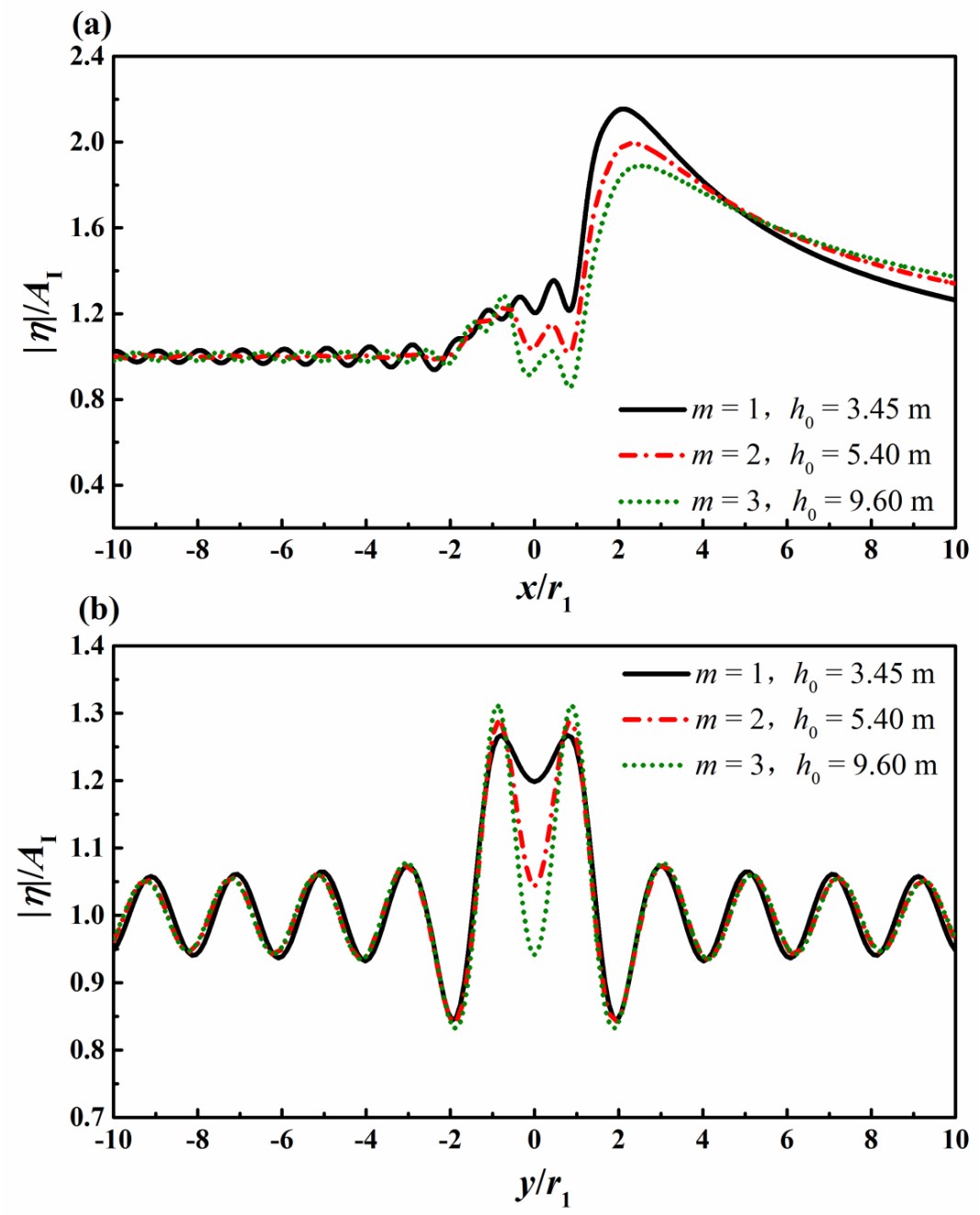
(a)
2.4
2.0
1.6
1.2
0.8
0.4
$|\eta|/A_1$
-10
-8
-6
-4
-2
0
2
4
6
8
10
x/r_1
$m = 1$, $h_0 = 3.45$ m
$m = 2$, $h_0 = 5.40$ m
$m = 3$, $h_0 = 9.60$ m
(b)
1.4
1.3
1.2
1.1
1.0
0.9
0.8
0.7
$|\eta|/A_1$
-10
-8
-6
-4
-2
0
2
4
6
8
10
y/r_1
$m = 1$, $h_0 = 3.45$ m
$m = 2$, $h_0 = 5.40$ m
$m = 3$, $h_0 = 9.60$ m

Figure 10

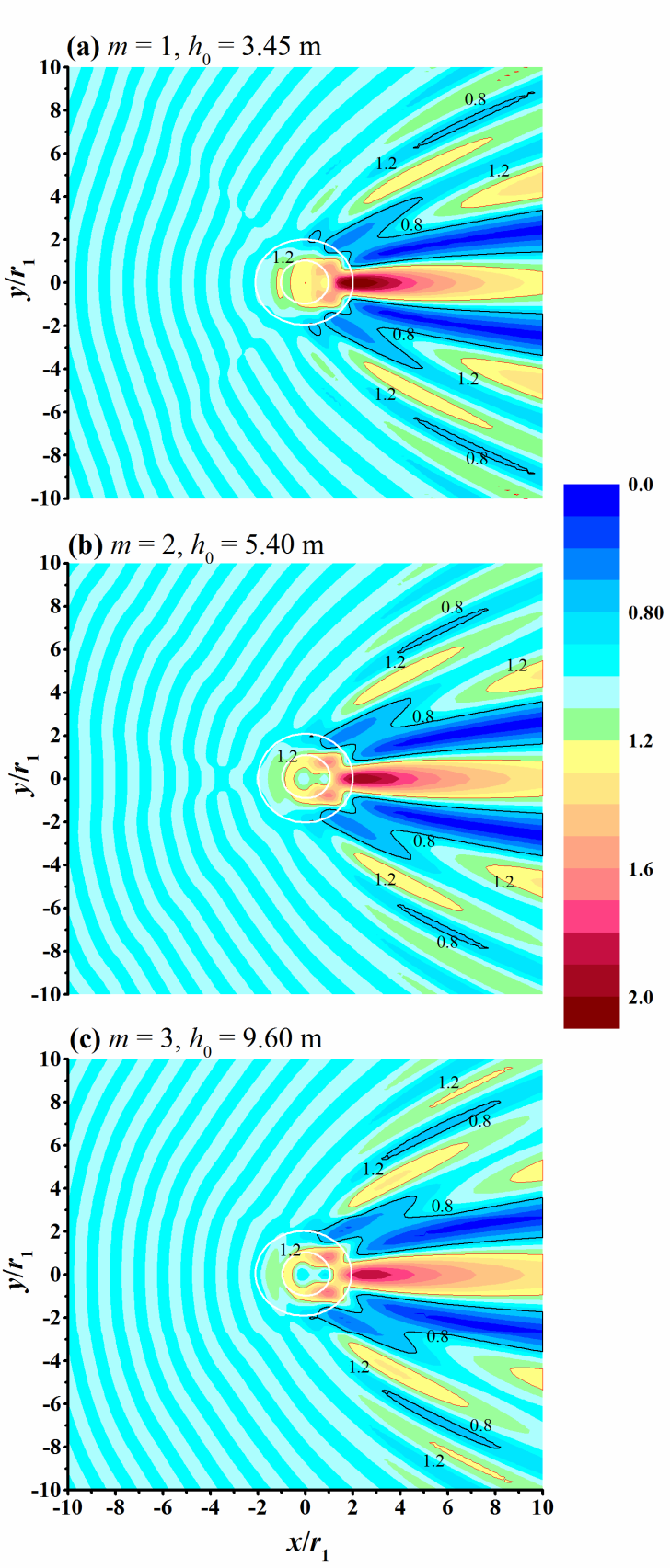

Figure 11

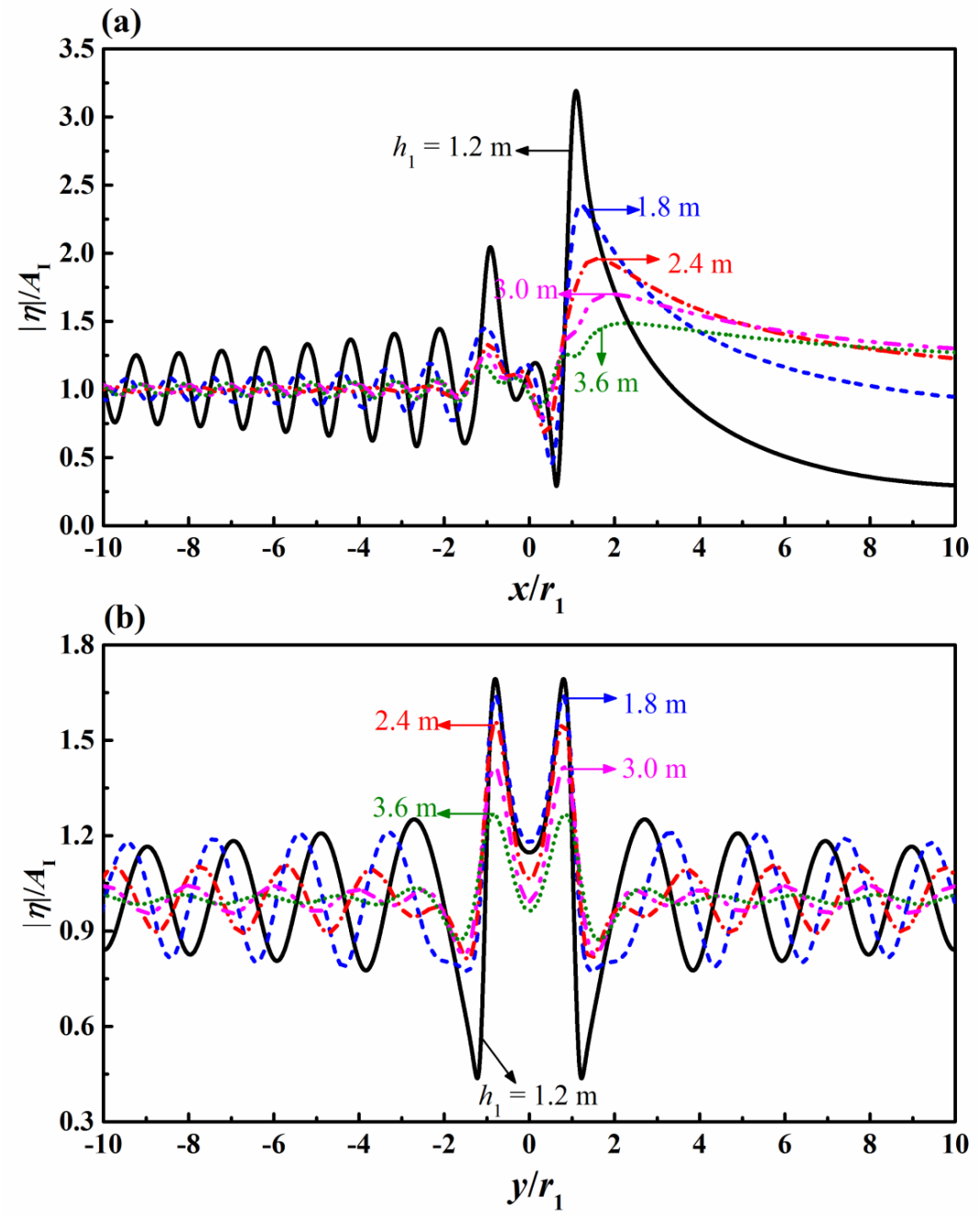
(a)
h_1 = 1.2 m
1.8 m
2.4 m
3.0 m
3.6 m
$|\eta|/A_1$
x/r_1
(b)
2.4 m
1.8 m
3.0 m
3.6 m
h_1 = 1.2 m
$|\eta|/A_1$
y/r_1

Figure 12